International Journal of Applied Earth Observation and Geoinformation 18 (2012) 232–242

Contents lists available at SciVerse ScienceDirect

International Journal of Applied Earth Observation and Geoinformation

journal homepage: www.elsevier.com/locate/jag

Mapping land subsidence in Jakarta, Indonesia using persistent scatterer interferometry (PSI) technique with ALOS PALSAR

Alex Hay-Man Ng[a,*], Linlin Ge[a,**], Xiaojing Li[a], Hasanuddin Z. Abidin[b], Heri Andreas[b], Kui Zhang[a]

[a] Geodesy and Earth Observing Systems Group (GEOS), School of Surveying and Spatial Information Systems, The University of New South Wales, Sydney, NSW, Australia
[b] Geodesy Research Division, Faculty of Civil and Environmental Engineering, Institute of Technology Bandung (ITB), Bandung, Indonesia

ARTICLE INFO

Article history:
Received 20 July 2011
Accepted 12 January 2012

Keywords:
Jakarta
Land subsidence
Displacement
SAR interferometry
Ground water extraction
GPS surveying
Persistent scatterer
PSI

ABSTRACT

Jakarta is the capital of Indonesia. It is one of the largest cities with an around 10 million population as for 2010, covering an area of about 661 square kilometers. The land subsidence phenomena in several areas of Jakarta are well known for many years. Land subsidence does damage infrastructures in the city; therefore, it has to be closely monitored and analysed. In this paper, the authors have demonstrated the capability of the PALSAR sensor aboard the Japanese ALOS satellite for large-scale mapping of land subsidence in Jakarta. Mapping results were produced from 17 ALOS PALSAR L-band radar images using persistent scatterer radar interferometry (PSI). The GEOS-PSI software, developed by the Geodesy and Earth Observing Systems group at UNSW for PSI analysis, was used to detect and map those land subsidence. The results showed that the land in the area of Jakarta was deforming at different rates across several zones. The land subsidence measured from ALOS PALSAR imagery were cross-examined with the subsidence values obtained from 4 GPS campaign surveys by the authors at 19 stations between 2007 and 2010. The magnitudes and trends of the deformation obtained from both techniques agreed well in general for those pinpoints of GPS. After the removal of 2 suspected outliers in GPS measurements, the subsidence rate difference between the two techniques range from −29 to 6 mm/year, with a standard deviation of 9 mm/year and an average absolute difference of 8 mm/year. This research has suggested that PSI with L-band ALOS PALSAR data can be a promising technique to complement the GPS surveying for monitoring land subsidence in super large cities like Jakarta.

© 2012 Elsevier B.V. All rights reserved.

1. Introduction

Land subsidence is a hazard resulting in negative impacts and could lead to serious problems, for example, increasing risk of flooding in coastal areas, cracking the buildings and infrastructures, destructing local groundwater systems, and generating tension cracks on land and reactivating faults (Primanita, 2010). Consequently, the necessity to monitor urban subsidence is understandable for the safety of the land surface users, as well as the management of urban planning.

Space-borne differential interferometric synthetic aperture radar (DInSAR) has proven to be an effective technique for land subsidence measurement due to its precision, spatial coverage and resolution. The capability of DInSAR for land deformation mapping has been demonstrated in many applications, for example, glacier movement (Kumar et al., 2011), volcanic activity (Lanari et al., 1998), crustal movement (Zebker et al., 1994; Zhang et al., 2010), and underground mining activity (Ge et al., 2007; Ng et al., 2009, 2010). Persistent/Permanent Scatterer Interferometry (PSI) is an extension of the conventional DInSAR techniques which aims to overcome the limitations of DInSAR by using multiple SAR image data to improve the detection ability for slow ground deformation (Ferretti et al., 2001). PSI carries out analysis on the backscattering objects of the ground surface that are coherent during the data acquisition period, known as persistent/permanent scatterers (PS). It is very important to identify these stable pixels because in the absence of a clear interferogram, these points may be sufficient to characterize the evolution of regional ground displacements. These backscattering objects can be found easily in the urban area, and hence PSI works well in urban environments such as Jakarta. The PSI techniques, developed by different investigators, have shown their potential for ground deformation monitoring in a number of applications, including deformation arising from urban subsidence (Chen et al., 2010; Osmanoglu et al., 2011), stability of infrastructure (Jiang and Lin, 2010), seismic faults (Massironi et al., 2009), volcanic activity (Hooper, 2006), and landslide prone slopes (Farina et al., 2006).

The land subsidence phenomenon in several areas in Jakarta is well known for many years (Abidin et al., 2008,

* Corresponding author. Tel.: +61 293854201.
** Corresponding author. Tel.: +61 293854177.
E-mail addresses: hayman.ng@gmail.com (A.H.-M. Ng), l.ge@unsw.edu.au (L. Ge).

0303-2434/$ – see front matter © 2012 Elsevier B.V. All rights reserved.
doi:10.1016/j.jag.2012.01.018

2001; Murdohardono and Sudarsono, 1998; Murdohardono and Tirtomihardjo, 1993). Land subsidence in Jakarta has been leading to severe damage to the buildings and infrastructures, increase in flooding areas, destruction to local groundwater systems, increased inland seawater intrusion. The land subsidence in Jakarta has been measured using the conventional surveying techniques, including levelling surveys, extensometer measurements, and GPS field surveys (Abidin et al., 2004). However, the measurements carried out by the conventional techniques in Jakarta were limited on specific points. Therefore, real subsidence phenomenon might not be observed. Since 2004, the subsidence phenomena in Jakarta also have been studied using DInSAR (Abidin et al., 2011). However since the deformation detecting ability of DInSAR is strongly influenced by the effect of atmospheric and decorrelation noise, and hence greatly reducing the precision of ground deformation detected (Ferretti et al., 2000, 2001). PSI technique thus is applied into Jakarta's study for the reasons of: (1) its ability to cover to a complete spatial extent and magnitude of deformation, (2) high mapping efficiency and cost-effective on labour for a large subsidence basin targeted, and (3) being able to obtain deformation measurements and its precision is comparable with conventional ground-based surveying techniques. The results of land subsidence in Jakarta City using PSI can provide critical information for flood risk assessment and management, hydrogeological assessment, groundwater extraction management, aquifer storage and recovery management, seawater intrusion assessment, and urban development planning.

This paper presents the land deformation over Jakarta, Indonesia obtained by using GEOS-PSI software to process L-band ALOS PALSAR radar imagery. Currently, data collected by the C-band SAR satellites, such as ERS-1/2, ENVISAT and Radasat-1, and the X-band SAR satellites, such as TerraSAR-X and COSMO-SkyMed, are often used in the PSI studies. Few studies have been carried out using the L-band SAR satellites such as ALOS PALSAR mainly because its relatively long wavelength (hence insensitive to displacement), long revisit cycle and insufficient number of archived data available. But in this study, the number of archived C-band SAR data over the test site Jakarta is too small for PSI analysis. On the other hand, there is sufficient number of archived L-band ALOS PALSAR data available for the land subsidence mapping over Jakarta. Therefore, the ALOS PALSAR data is used in this study and its capability for persistent scatterer radar interferometry (PSI) to map the land subsidence is investigated herein as well.

This paper is organised as follows. The location and geological settings of Jakarta are presented in Section 2. Section 3 is describing the used of GEOS-PSI to estimate the linear and non-linear term displacement parameters. The results obtained from GEOS-PSI software over Jakarta using ALOS PALSAR data is then presented in Section 4. The results are then compared with the GPS surveys data by Section 5. In Section 6, the analysis of the reasons for the dispersion between both techniques is provided. Subsequently, the measurements from both techniques are discussed. Finally, some concluding remarks are presented.

2. Study area and data availability

Jakarta is the capital city of Indonesia. It is the largest city in Indonesia and located on the northwest coast of Java, covering an area of about 661 square kilometers (Fig. 1). The total population of Jakarta is approximately 10 million as of 2010 (Setiawati, 2010). Jakarta is set in a lowland area which is relatively flat. The topographical slopes in the northern and central parts of Jakarta range between 0° and 2°. The ranges of the topographical slopes are slightly larger in the southern parts which are between 0° and 5°. Jakarta has five main landforms (Rimbaman and Suparan, 1999): alluvial, marine-origin, beach ridge, swamp and mangrove swamp landforms, and former channels. It should be noted that there are about 13 natural and artificial rivers flowing through the city, some of which are used for supplying water to the public.

The population density in Jakarta and its surrounding areas has grown rapidly in the last three decades due to the urban development and the demands of a growing population. Land subsidence is one of the consequences due to the urban development in Jakarta. It has been reported in many studies (Abidin et al., 2008, 2001; Primanita, 2010) that the land subsidence in Jakarta was the result of: (1) over-extraction of groundwater, (2) extensive conversion of prime agricultural areas into residential and industrial, (3) massive construction, (3) natural consolidation of soil layers and (4) tectonic movements. The deformation measured by PSI can provides more information to aid understanding of the causes land subsidence phenomenon in Jakarta.

3. Methodology – PSI for land deformation mapping

In this study, GEOS-PSI (Ng et al., 2012) was used to produce the map of land subsidence in Jakarta and its surrounding region. A total of 17 L-band ALOS PALSAR images acquired from 31 January 2007 to 26 September 2010 over Jakarta were used in this study. A single reference (master) image was selected for the generation of interferogram stack. The chosen master image in this study was acquired on 3 February 2008 with shortest perpendicular and temporal baselines corresponding to other images. The perpendicular baseline and the temporal baseline of all images with respect to the image acquired on 3 February 2008 is shown in Fig. 2. Sixteen differential interferograms were generated with respect to the master image using the conventional 2-pass DInSAR approach (Massonnet et al., 1993). A three arc-second Shuttle Radar Topography Mission (SRTM) Digital Elevation Model (DEM) was used for removing topography phase from the interferograms.

3.1. Differential interferometric phase for ground displacement detection

When talking about the phase of radar image, it is the state of vibration of the radar wave at the instant that it is received by the radar system. It completes a journey comprising an integer number of wavelengths in a returned trip. The phase of a radar image is therefore only meaningful when compared with that of a second one. The two images which are merged point by point to form the interferogram with the phase differences. The phase variation in the differential interferograms contained information of the surface displacement, DEM error, atmospheric error (or inhomogeneities if its effect is ignored), and residual orbital errors which can be written as:

$$\phi = \phi_{\text{Topo}} + \phi_{\text{Defo}} + \phi_{\text{Atmos}} + \phi_{\text{Orbit}} + \phi_{\text{Noise}} + \phi_{\text{az}} - 2\pi n \quad (1)$$

where ϕ is the phase variation in the differential interferogram, ϕ_{Topo} is the phase due to the DEM error, ϕ_{Defo} is the phase due to the geometric displacement of the point between the two image acquisitions, ϕ_{Atmos} is the phase due to atmospheric disturbances, ϕ_{Orbit} is the phase due to residual orbital error, ϕ_{Noise} is the phase due to noise, ϕ_{az} is the interferometric phase related to the azimuth sub-pixel position with respect to the centre of the resolution cell, and n is an integer ambiguity number. The model for the differential interferometric phase of image acquisition n with respect to the master image for a point x in Eq. (1) can be written as (Hanssen, 2001; Hooper, 2006):

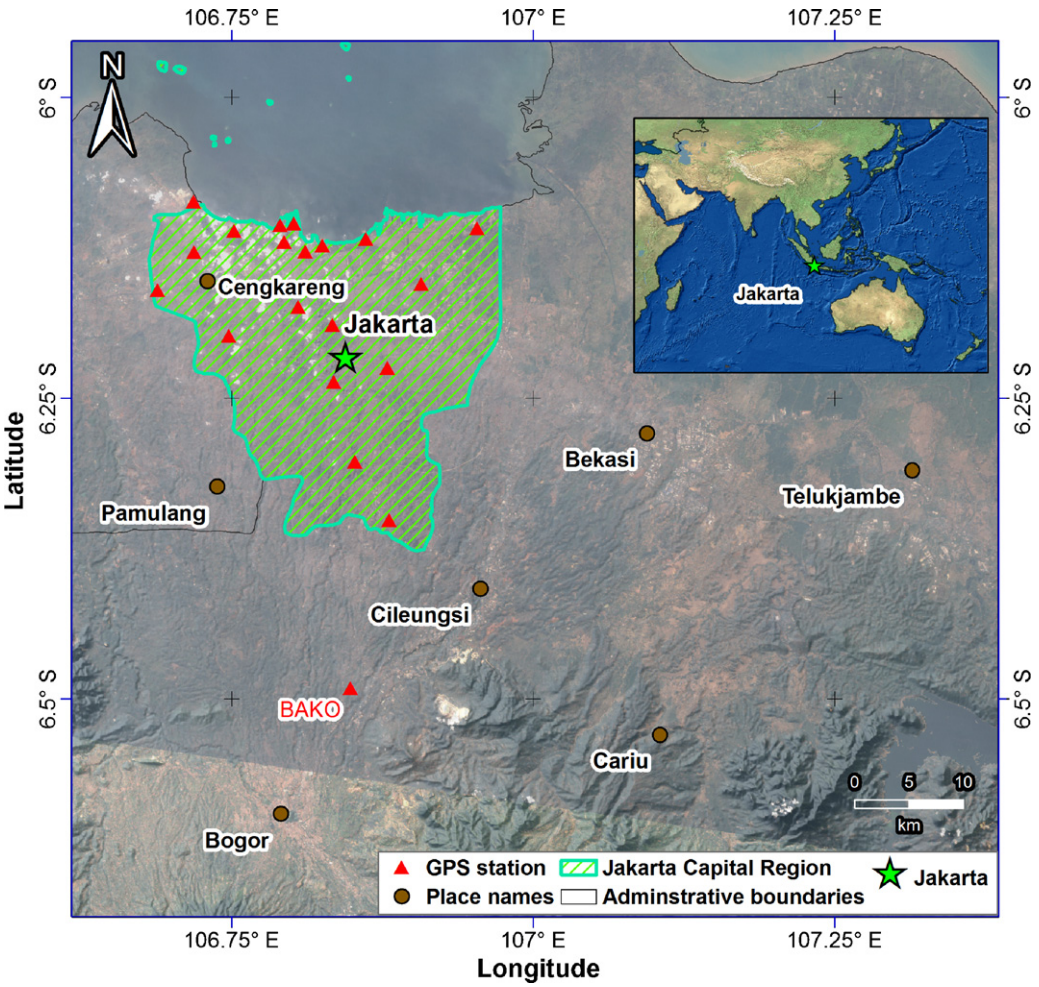

Fig. 1. Jakarta basin and its surrounding. The red triangle next to BAKO is the location of GPS reference stations. (For interpretation of the references to colour in this figure legend, the reader is referred to the web version of this article.)

$$\Delta\phi_x^n = W\left\{-\frac{4\pi}{\lambda}\Delta R_x^n - \frac{4\pi}{\lambda}\frac{\Delta h_x}{R_{1,x}\ \sin\theta_x^0}B_{\perp,x}^n + \eta_x^n \cdot az_x + \phi_{\text{Atmos},x}^n + \phi_{\text{Orbit},x}^n + \phi_{\text{Noise},x}^n\right\} \quad (2)$$

where $W\{\cdot\}$ is the wrapping operator which indicates that the differential interferometric phase $\Delta\phi_x^k$ is modulo-2π. The first term is the phase due to deformation of the pixel in the time between the image acquisitions. Giving that multiple interferograms are available, the deformation of the pixel along the interferometric stack can be decomposed as:

$$\Delta R_x^n = v_x \cdot T^n + d_x^n \quad (3)$$

where $v \cdot T^n$ is the slant range linear deformation that occurs between the date of the image acquisition n and the master image, v is the constant slant range velocity of deformation along the interferometric stack, T^n is the temporal baseline between image acquisition n and the master image, and d^n is the non-linear deformation term. The second term represents the phase due to DEM error. The DEM error Δh at the stable scatterer is assumed to be the same along the interferogram stack, hence the phase due to DEM error is depending mainly on the local perpendicular baseline. The third term is the Doppler centroid phase term, which is related to the azimuth sub-pixel position with respect to the centre of the resolution cell, az. It is depended on the difference in Doppler centroid frequency between image acquisition n and master image and the instantaneous velocity of the satellite at the pixel in an earth-fixed coordinate system. η_x^n denotes the azimuth sub-pixel position coefficient (Kampes, 2005). In this study, the ALOS PALSAR data are focused to a common Doppler centroid, therefore the azimuth sub-pixel position component was not considered here.

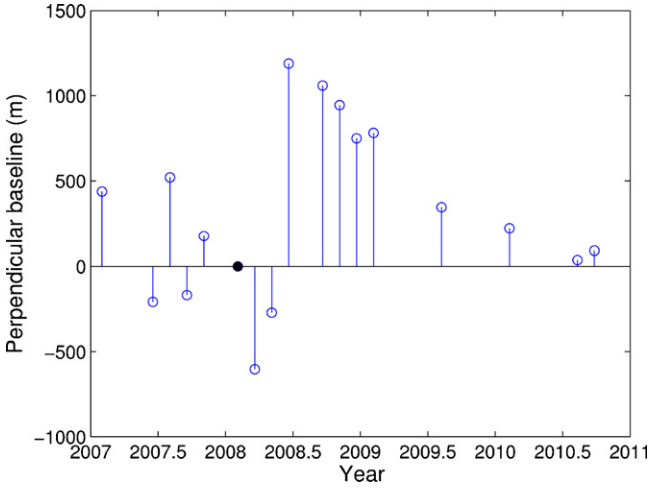

Fig. 2. Baseline distribution of available ALOS PALSAR data for Jakarta area (Orbit direction: Ascending; Path: 437; Frame: 706; Incidence angle: ~38.7°; Look direction: Right; Polarisation: HH).

3.2. Persistent scatterer candidate (PSC) selection

PSI carries out analysis on the PS points. It utilises the phase information at the PSs, backscattering objects that are coherent along the image stack, in order to measure the displacement time series at the PSs. In this study, the amplitude dispersion index (D_A) (Ferretti et al., 2001) was used to estimate the phase stability of the pixels and to detect PSC. The calculation for the amplitude dispersion index of each pixel was performed. Pixels with lower D_A are expected to be more reliable as they have higher chance to be a PS pixel. Pixels with $D_A < 0.25$ are assumed to be reliable and are used to construct the reference network. The network was constructed based on Delaunay triangulation network with a maximum arc length of 1.5 km.

3.3. Phase unwrap model and parameters estimation

By considering the phase differences $\Delta\phi^n_{x,y} = \Delta\phi^n_y - \Delta\phi^n_x$ between neighbouring pixels, pixels x and y, at interferogram n, the phase model of an arc (the path corresponding to pixels x and y) along the interferogram stack can be considered to be a linear system of equations (Kampes, 2006):

$$\begin{bmatrix} \Delta\phi^1_{x,y} \\ \Delta\phi^N_{x,y} \end{bmatrix} = \begin{bmatrix} -2\pi & & \\ & \ddots & \\ & & -2\pi \end{bmatrix} \cdot \begin{bmatrix} a^1_{x,y} \\ \vdots \\ a^N_{x,y} \end{bmatrix} + \begin{bmatrix} -\frac{4\pi}{\lambda} T^1 & -\frac{4\pi}{\lambda} \frac{B^1_{\perp,x,y}}{R_{1,x,y} \sin\theta^0_{x,y}} \\ \vdots & \vdots \\ -\frac{4\pi}{\lambda} T^N & -\frac{4\pi}{\lambda} \frac{B^N_{\perp,x,y}}{R_{1,x,y} \sin\theta^0_{x,y}} \end{bmatrix} \cdot \begin{bmatrix} v_{x,y} \\ \Delta h_{x,y} \end{bmatrix} + e \quad (4)$$

where $B^n_{\perp,x,y}$, $R_{1,x,y}$, $\theta^0_{x,y}$ and $a^n_{x,y}$ is the mean perpendicular baseline, range distance, local incidence and the integer ambiguity value, respectively. $v_{x,y}$ and $\Delta h_{x,y}$ is the difference in displacement rate and DEM error, respectively. The residual vector e consists of unmodelled errors. The modelled parameters for each arc of the triangulation (i.e. $v_{x,y}$ and $\Delta h_{x,y}$) were estimated using the Integer Least Square (ILS) estimator with LAMBDA method (Kampes and Hanssen, 2004). The absolute 'ensemble phase coherence' (Ferretti et al., 2001), $|\gamma|$, was used to determine the goodness-of-fit for the modelled parameters estimated from each arc. The arcs with $|\gamma|$ lower than 0.85 were removed.

Once the modelled parameters differences of all arcs in the reference network were estimated, the absolute modelled parameters (i.e. displacement rate and DEM error) for each pixel could be computed. A robust least squares estimation scheme (called M-Estimation) was performed for spatial integration and to detect the outliers in order to estimate the absolute modelled parameters. The weight function used in this study was the Tukey's bisquared function (Tukey, 1977) with tuning constant $c = 4.685$.

In order to maximise the number of pixels detected by the PSI analysis, the less reliable PSCs were also analysed. In this study, only the pixels with $D_A < 0.4$ were analysed due to the large data size of a full scene ALOS PALSAR image. An adaptive estimation strategy was performed to estimate the parameters of these PSCs (Ng et al., 2012). The adaptive estimation strategy can be separated into two different parts: (1) using an adaptive window to add an individual pixel into the reference network and (2) to prioritise the order of pixels to be added into the reference network. A detailed description of the adaptive estimation strategy can be found in (Ng et al., 2012).

3.4. Atmospheric signal estimation and removal

After calculating the modelled parameters for the PSC, the unwrapped model phase for each PSC in all the interferograms was calculated. The phase residual $\Delta\phi^n_{\text{Residual}}$ was calculated by subtracting the unwrapped model phase $\Delta\phi^n_{\text{Model}}$ from the original differential interferometric phase $\Delta\phi^n$:

$$\begin{aligned} \Delta\phi^n_{\text{Residual},x} &= W\{\Delta\phi^n_x - \Delta\phi^n_{\text{Model},x}\} \\ &= W\{\phi^n_{\text{Nonlinear},x} + \phi^n_{\text{Atmos},x} + \phi^n_{\text{Orbit},x} + \phi^n_{\text{Noise},x}\} \end{aligned} \quad (5)$$

where x stands for the selected pixel. The residual phase at the selected pixels in each interferogram contains four phase components: the non-linear displacement $\phi^n_{\text{Nonlinear}}$, the atmospheric disturbance (or error) ϕ^n_{Atmos}, the orbital error ϕ^n_{Orbit}, and the noise ϕ^n_{Noise}. In order to simplify the calculation, the orbital error component was considered to be part of the atmospheric phase component (Ferretti et al., 2000). The residual phases for each interferogram were first unwrapped by the sparse Minimum-Cost Flow (MCF) unwrapping algorithm (Costantini and Rosen, 1999). In this study, the topography and non-topography related atmospheric signals were treated separately. The topography related atmospheric signals in each differential interferogram were estimated based on the linear relationship between the pixels' elevation (i.e. DEM height + DEM error) and their unwrapped residual phase using the M-Estimation method. The non-topography related atmospheric signals were estimated from the refined unwrapped residual phases (i.e. after the removal of the phase component due to topography related atmospheric signal) based on the low pass filtering operation in spatial domain and high pass filtering operation in the temporal domain (Ferretti et al., 2001). In this study, the displacement, DEM error and atmospheric components were iteratively updated until these components hardly affect the number of accepted pixels and the displacement estimates.

3.5. Linear and non-linear displacement estimation

Once the modelled parameters and atmospheric signals were estimated, the residuals phases were calculated by removing the phase contribution due to modelled parameters and atmospheric signals from the differential phase from each interferogram. The residual phases were expected to contain two components: non-linear displacement (d^n) and error. In this study, a low-pass filtering operation in spatial domain was carried out to estimate the non-linear displacement component.

The displacement values measured from SAR are along the radar Line-of-Sight (LoS) direction. Therefore the displacement measured from SAR is a composite of vertical, easting and northing displacement components, which can be expressed as (Fialko et al., 2001):

$$\begin{bmatrix} \cos(\theta) & -\sin(\theta)\cos(\alpha) & \sin(\theta)\sin(\alpha) \end{bmatrix} \begin{bmatrix} D_U \\ D_E \\ D_N \end{bmatrix} = D_{\text{LoS}} \quad (6)$$

where θ is incidence angle at the reflection point, α is azimuth of the satellite heading vector (positive clockwise from North), D_U, D_E and D_N are the displacement in vertical, easting and northing directions, respectively. D_{LoS} is ground displacement in the LoS direction between two acquisitions. Due to the lack of different viewing geometry, it was not possible to resolve the 3D displacement vectors in this study. It is assumed that the deformation in Jakarta City was mainly in vertical direction and hence the LoS displacement

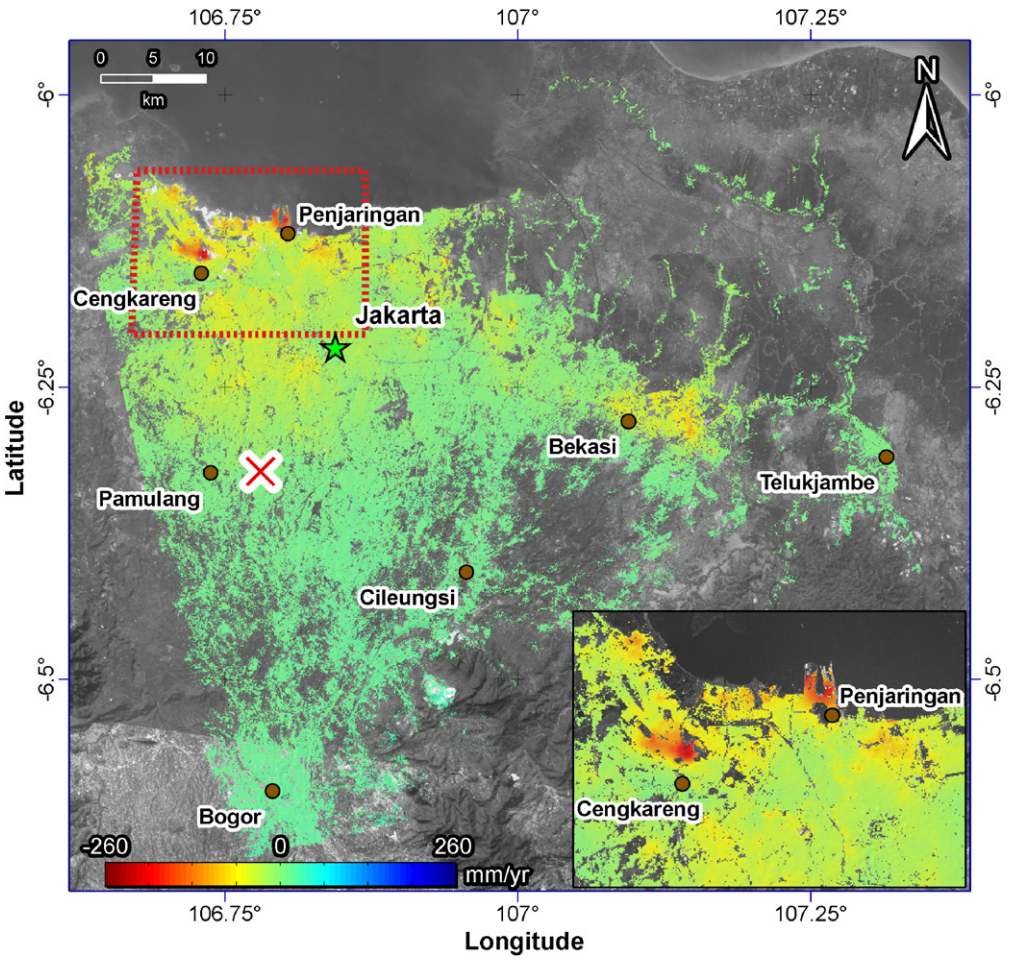

Fig. 3. Measured subsidence rate from ALOS PALSAR data (Path 437) superimposed on the Landsat 5 image of Jakarta metropolitan and its surrounding. The close-up image (highlighted by the red broken line) is shown at the bottom right. The red cross represents the location of the reference point. The negative value indicates the ground surface is subsiding and the positive value indicates the ground surface is uplifting. (For interpretation of the references to colour in this figure legend, the reader is referred to the web version of this article.)

measured from PSI was directly projected into the vertical direction assuming that there was no displacement in horizontal direction.

4. Results: Measurements of land subsidence in Jakarta from PSI

Seventeen ALOS PALSAR images acquired over Jakarta from 31 January 2007 to 26 September 2010 from an ascending orbit were analysed using PSI. There were 17,625,508 PSCs selected for the PSI analysis (i.e. PSCs with $D_A < 0.40$), where 789,847 of the PSCs were used to create the initial reference network (i.e. PSCs with $D_A < 0.25$). The reference pixel was chosen in the southern end of Jakarta at the east of Pamulang (marked by the red cross in Fig. 3). The area surrounding the reference pixel selected was relatively flat and without high-rise buildings. The displacement values derived from the PSI results were relative to the reference point. After the PSI analysis, a total of 4,785,612 PS pixels were identified, of which 699,126 PS pixels have $D_A < 0.25$. The subsidence rate map generated with the ALOS PALSAR data is shown in Fig. 3. The results showed that the land in the area of Jakarta was deforming at different rates ranging between −260 mm/year (subsiding) and 100 mm/year (uplifting). It can be seen that the subsidence mainly occurred inside the Jakarta and Bekasi. There are two noticeable subsidence bowls located at the Jakarta along the coastal area and lowland area in northwestern Jakarta (around Penjaringan and Cengkareng). Subsidence rates up to 260 mm/year have been observed at the two subsidence bowls. Several other subsidence bowls with relatively lower subsidence rate have also been observed in the other parts of the Jakarta metropolitan area as well as Bekasi metropolitan area. The observed subsidence rates at the Bekasi metropolitan area are as high as 115 mm/year. It can be seen in Fig. 3 that very few PS pixels were identified over the agriculture and vegetated area at the East of Jakarta and the mountains area (with vegetation) at South East of the Jakarta. The land cover over these areas is expected to vary with time and for this reason very few PS pixels can be identified. The subsidence time series for 9 selected dates are shown in Fig. 4. It can be seen that the land deformation in Jakarta is mostly continuous along the time. There are no obvious sudden changes in deformation trend observed. As shown in Fig. 4, the magnitude of the land subsidence inside the Jakarta and Bekasi increased rapidly. The land over two obvious subsidence bowls in Jakarta (appears as two red dots in Fig. 4i) have subsided up to 865 mm between 31 January 2007 and 26 September 2010 (about 1334 days).

5. Comparison with GPS surveys

In order to evaluate the accuracy of the PSI-measurements, the results should be compared with the deformation obtained from other techniques. In this study, the PSI results were compared against GPS surveys to quantitatively validate the results obtained.

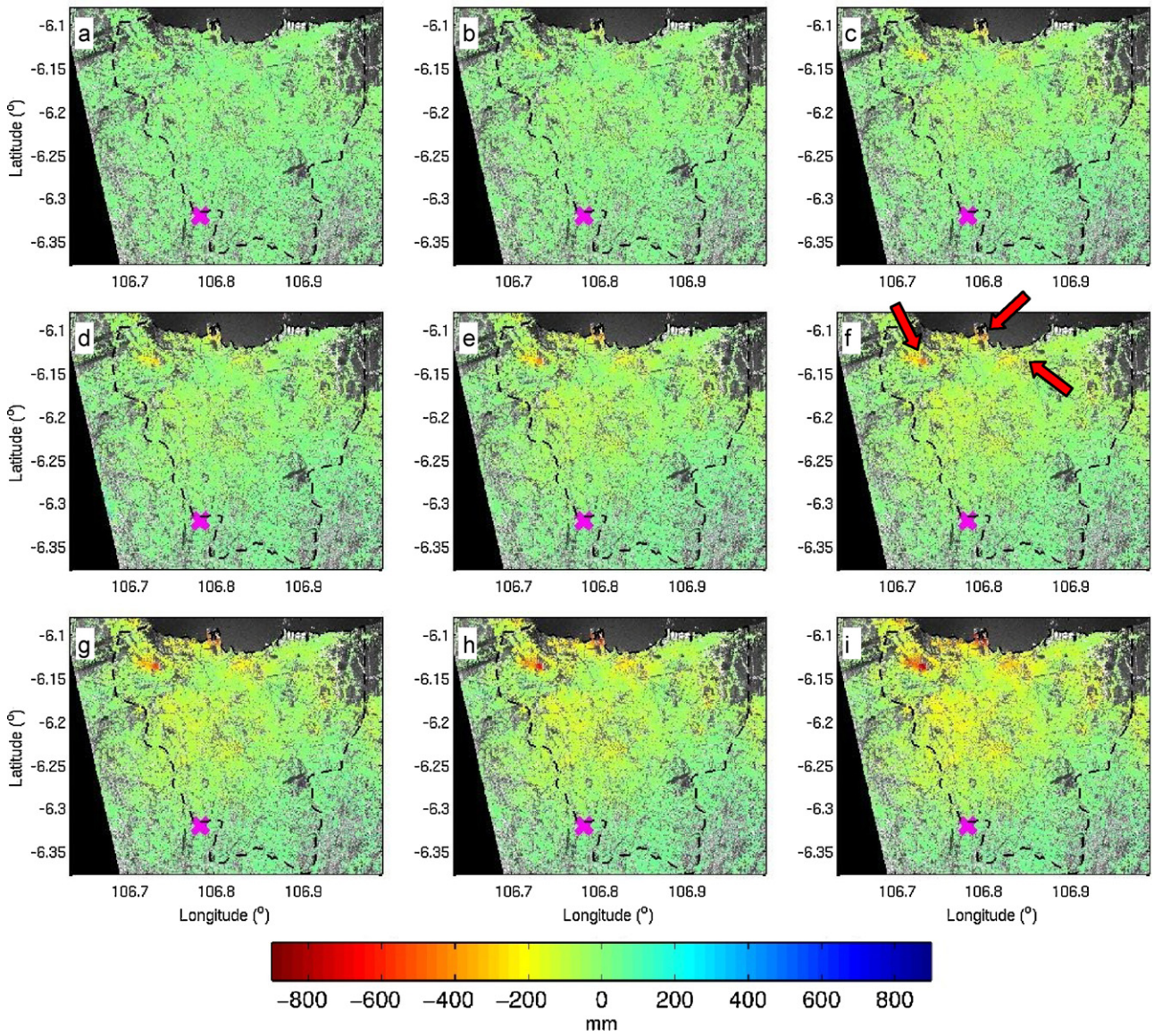

Fig. 4. PSI-measured subsidence time series at Jakarta region with respect to 31 January 2007 for 9 selected dates on: (a) 18 June 2007, (b) 18 September 2007, (c) 20 March 2008, (d) 20 June 2008, (e) 21 December 2008, (f) 05 February 2009, (g) 08 August 2009, (h) 08 February 2010 and (i) 26 September 2010. The three arrows in (f) indicate the location of the three largest subsidence bowls. The black broken line indicates the administrative border of Jakarta. The magenta cross represents the location of the PSI reference point. (For interpretation of the references to colour in this figure legend, the reader is referred to the web version of this article.)

5.1. GPS surveys for land subsidence study in Jakarta from 2007 to 2010

The development of land subsidence over Jakarta has been monitored by GPS surveying at 36 stations. Since January 2006, 4 GPS surveys have been conducted by the Geodesy Research Division of Institute of Technology Bandung (ITB) in 3–7 September 2007, 22–31 August 2008, 15–20 July, 2009, and 9–21 May 2010. However, the surveys did not always occupy the same stations. There are only 19 stations with GPS surveying carried out in all four campaigns. Therefore only the data from these 19 stations were used in this study. The location of the 19 GPS benchmarks used in this study is shown in Fig. 1 (red triangles). The GPS survey data were collected using the dual-frequency geodetic-grade GPS receivers. The length of the observation sessions was around 9–11 h. The data were collected at 30 s intervals using an elevation mask of 15°. The GPS survey data were analysed as described in Abidin et al. (2008). The GPS station "BAKO" at the southernmost point in the network (labeled by the text in red colour in Fig. 1) was used as the reference stations and all ellipsoidal heights of all stations are relative to the reference stations.

The comparison between PSI and GPS measurements was carried out in two ways to compare: (1) the subsidence rate and (2) the displacement time series of each station obtained from both measurements.

5.2. Comparison with GPS-derived subsidence rate

Fig. 5 shows the subsidence rates in Jakarta derived from the GPS data. The subsidence rate based on the GPS data were calculated from the GPS displacement time series using the least square approach. By comparing Figs. 3 and 5, the deformation patterns and magnitudes estimated from both measurements agree well with each other.

A quantitative analysis of the differences between subsidence rates obtained from both measurements was performed for the validation purpose. It is worth noting that the PSs for PSI-measurements and permanent marks for GPS surveys are often at

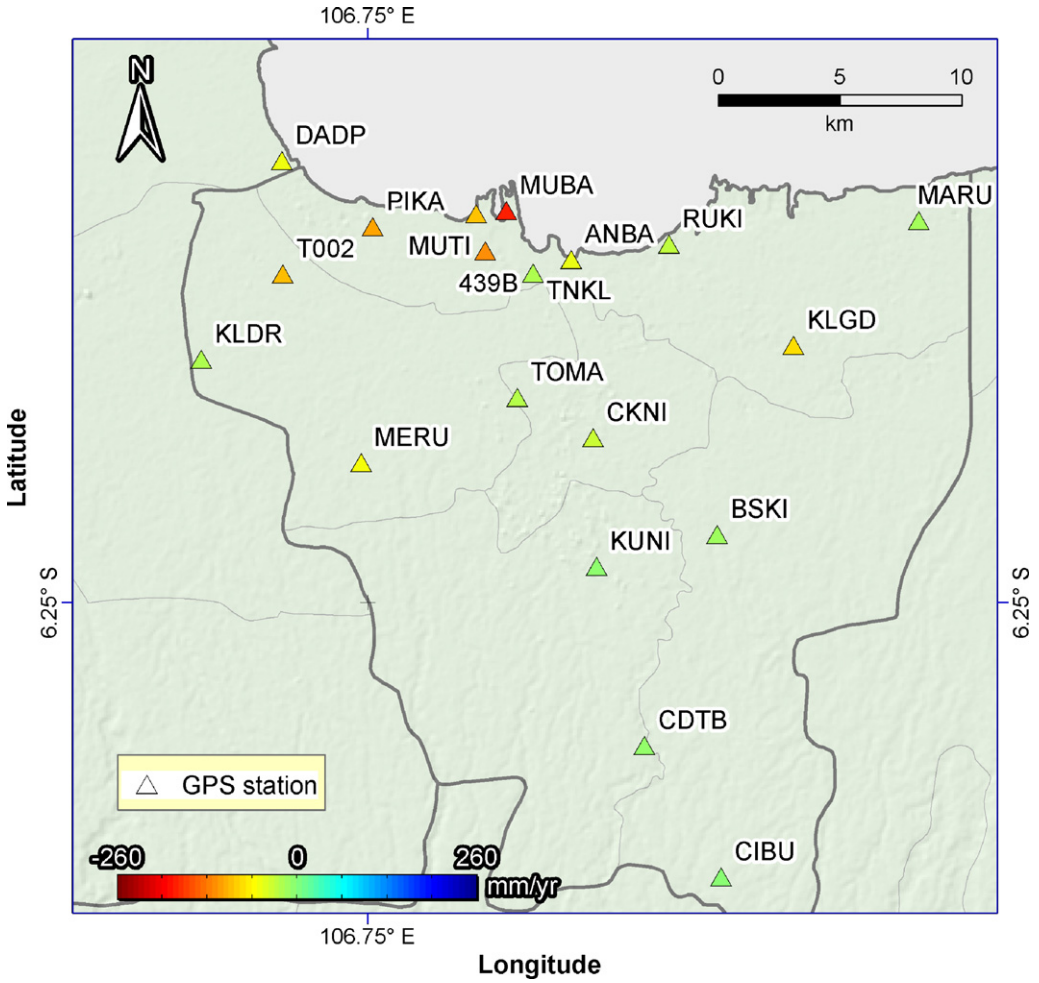

Fig. 5. Rates of land subsidence in Jakarta monitored by the GPS network.

difference locations. In order to match the identified PS and the GPS stations, the following procedure was applied:

(1) A map with 100 m × 100 m grid was created.
(2) The location of the PSs corresponding to the map was assigned (usually multiple PSs within a grid).
(3) The location of the GPS stations corresponding to the map was identified.
(4) The PSs at the same grid of the corresponding GPS stations (closest) were removed if the elevation difference between the PS (i.e. DEM height + DEM error) and the GPS stations was more than 10 m.
(5) The displacement values of each grid were calculated by averaging the remaining PSs corresponding to the grid.

The points obtained applying the above procedure were assumed to be the same scatterers between measurements, or at least had a common deformation signal.

A histogram of the subsidence rates differences between both techniques is shown in Fig. 6. The PSI-measured subsidence rates were calculated with respect to the GPS station "BAKO". The differences vary from −29 mm/year to 38 mm/year, the average absolute difference is 11 mm/year and the standard deviation is 16 mm/year. It can be seen in Fig. 6 that differences at two stations ("KLGD" and "439B") were abnormally large. This is most likely because the PSs obtained from the PSI-measurement were not measuring the same backscattering objects corresponding to the two GPS stations. Therefore measurements from the two GPS stations ("KLGD" and "439B") were considered as outliers and were removed from further analysis. After the removal of the two GPS stations, the average absolute difference is improved to 8 mm/year and standard deviation was 9 mm/year.

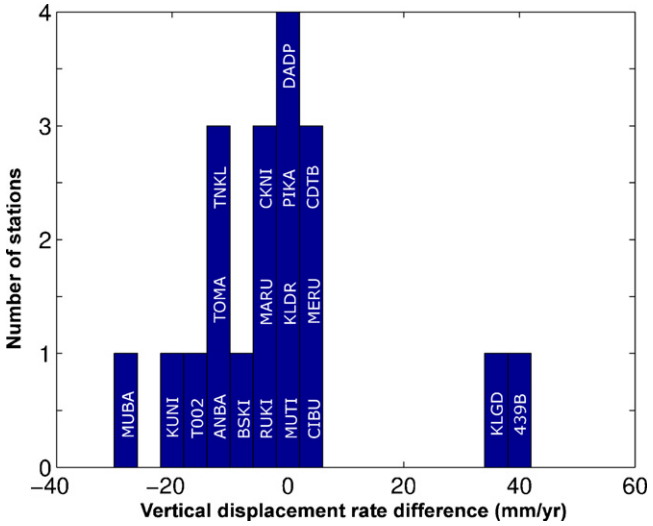

Fig. 6. The distribution of displacement rate difference between the PSI-measurement and GPS-measurement. The GPS stations corresponding to each bin are written in white in the histogram.

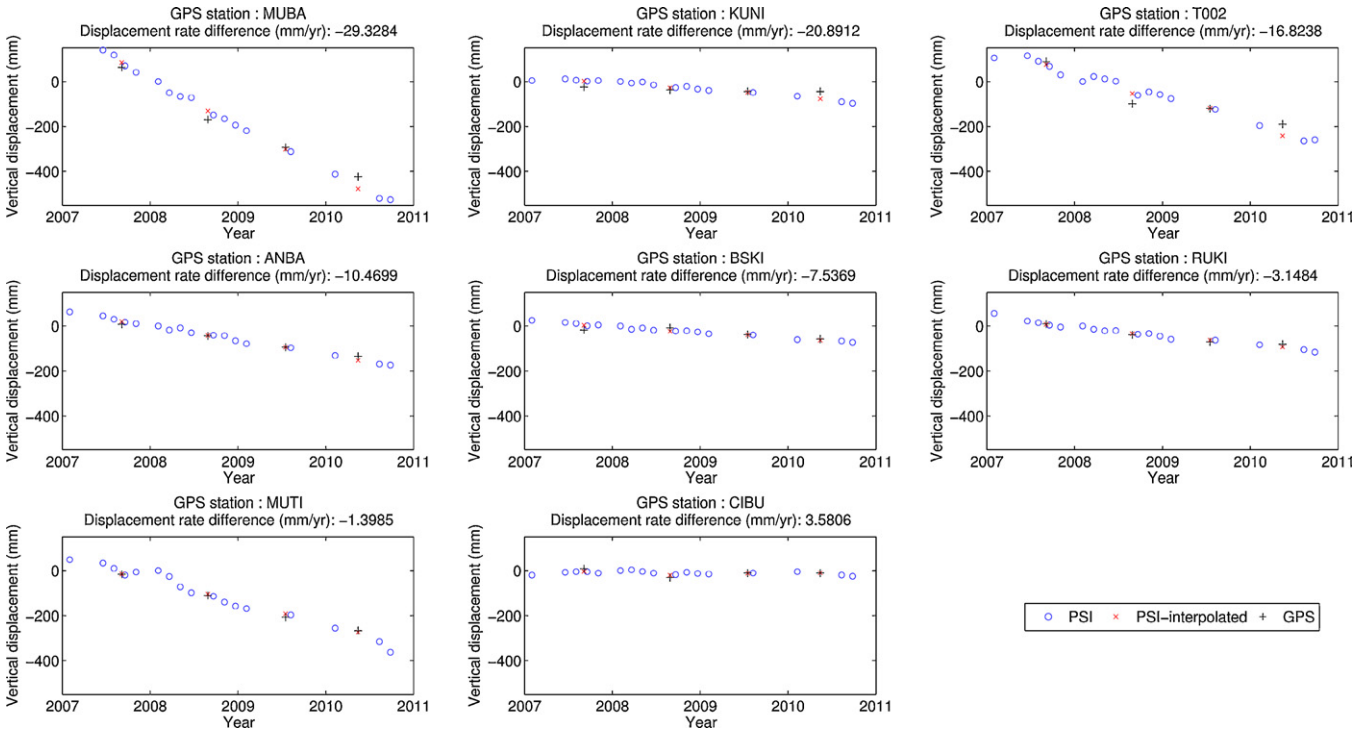

Fig. 7. Comparison between PSI-measured vertical displacement and GPS-measured vertical displacement time series at the GPS survey points "MUBA", "KUNI", "T002", "ANBA", "BSKI", "RUKI", "MUTI" and "CIBU". The circles, crosses and plus signs represent the PSI-measurements, PSI-interpolated deformation and the GPS-measurements, respectively. The displacement values are calculated with respect to the GPS station "BAKO" and the acquisition date of the reference ALOS PALSAR image (i.e. 3 February 2008).

5.3. Comparison with GPS-measured displacement time series

The comparison between GPS-measured and PSI-measured displacement time series was made by recalculating the PSI displacement time series with respect to the reference GPS station ("BAKO") so as to compare with the corresponding GPS-measurements. A strong correlation has been observed between the GPS-measured and PSI-measured displacement time series. Fig. 7 shows the measured deformation histories for 8 selected GPS stations from which one GPS station in each discrete interval (bin) of the histogram shown in Fig. 6 is selected for the comparison. It can be seen that the displacement time series obtained from both measurements match reasonably well. Seasonal displacements have been also observed from the PSI-measured displacement time series. It is important to note that the temporal sampling rate of the GPS campaign surveys is much lower than the SAR acquisitions (Fig. 7). In order to quantitatively compare the displacement time series measured from both techniques, cubic spline interpolation was carried out on the PSI-measurement in the time domain. The PSI-measured displacement time series corresponding to the GPS stations were interpolated to the dates of the GPS surveys. The centre date of each GPS survey period was taken as the date of the GPS survey campaigns. The comparison between the PSI-interpolated displacement time series and the GPS-measured displacement time series for all GPS stations is shown in Fig. 8. The differences vary from −54 mm to 45 mm, the average absolute difference is 14 mm and the standard deviation is 19 mm. The correlation coefficient of fit, r^2, for the comparison is 0.92.

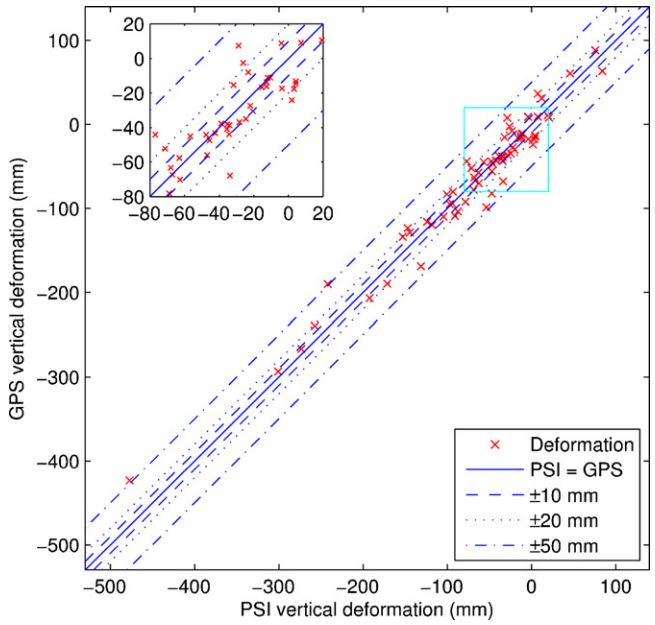

Fig. 8. Comparison between interpolated PSI-measured vertical displacement and GPS-measured vertical displacement at the GPS survey points. The displacement values are calculated with respect to the GPS station "BAKO".

6. Discussion

6.1. Reliability of L-band ALOS PALSAR PSI results

The comparison with GPS measurements has demonstrated the reliability of PSI results. It is expected that the differences between the two techniques were mainly caused by several reasons discussed below.

6.1.1. Errors in the PSI measurement

The accuracy of the PSI estimated LoS displacement rate depends on wavelength of the sensor, temporal baseline

distribution and phase stability of the target. The ALOS PALSAR data used in this study was acquired by L-band sensor which is less sensitive to deformation compared to C-band and X-band sensors. The expression for the variance of error for LoS displacement rate estimates from PSI is approximately valid (Colesanti et al., 2003; Ferretti et al., 2000):

$$\sigma_v^2 = \frac{\lambda^2 \sigma_\phi^2}{(4\pi)^2 \sum_{n=1}^{N} (T_n - \bar{T})^2} \tag{7}$$

where σ_v and σ_ϕ are the standard deviation of estimated deformation rate and phase residuals, respectively. T_n is the date of the image acquisition n and $\bar{T}$ is the average temporal baselines. Based on Eq. (7), the standard deviation of error for the PSI-derived LoS displacement rate can be derived:

$$\sigma_v = \frac{\lambda \sigma_\phi}{4\pi \sqrt{N} \sigma_T^2} \tag{8}$$

where σ_T is the standard deviation of the temporal baseline. Given a fixed phase residual and temporal baseline distribution, the precision of displacement measurement for the L-band datasets (e.g. ALOS PALSAR) is approximately 4.2 and 7.6 times worse than the counterpart for the C-band datasets (e.g. ENVISAT ASAR) and X-band datasets (e.g. TerraSAR-X), respectively. Therefore the PSI results measured from ALOS PALSAR dataset was expected to be less precise than the datasets acquired by the C-band (e.g. ENVISAT, Radarsat-1/2) and X-band satellites (e.g. TerraSAR-X and COSMO-SkyMed).

In addition, the precision of the PSI results are strongly influence by the number of interferograms available. In this study, only 17 ALOS PALSAR data were available.

With such a small datasets, it is possible that the phases of the incoherent backscattering objects by chance fit well with the displacement model. These pixels could be wrongly interpreted as PSs and hence affected the precision and reliability of the PSI measurements.

6.1.2. Reliability of the GPS measurements

In this study, the GPS stations cannot always be established in a desired location in every survey due to two reasons: (1) the signal obstruction and multipath caused by high rise buildings, trees, billboards, etc. and (2) active development activities inside urban areas, which sometimes destroy or alter observation monuments. The reference GPS station "BAKO" is located about 17 km away from the closest GPS station in the Jakarta capital region and 50 km away from the GPS station on the coast. In order to minimise atmospheric effects and achieve the best possible differential GPS accuracy, baselines between the reference and rover stations should be as short as possible, e.g. between 10 and 15 km. The expected standard deviations of the GPS-derived relative ellipsoidal heights from all surveys were in general about 10 mm (Abidin et al., 2008). Furthermore, there were a few points with larger stand deviation, due to the lack of observation data caused by signal obstruction. The accuracy of the episodic GPS measurements used in this study is relatively poorer compared to the measurements from the continuous operating GPS network. Therefore, the inaccuracy in GPS measurements could be another reason for the dispersion in deformation measured with both techniques.

6.1.3. Existence of horizontal displacements

The existence of horizontal displacements, which were assumed negligible, could impact the reliability of the PSI measurements. Several subsidence bowls with magnitude over 50 mm/year can be observed in Figs. 3 and 4. Although the land deformation in Jakarta was expected mainly occurred in vertical direction, small amount of horizontal displacement was expected especially near the rim of the subsidence bowls. The horizontal displacement could reduce the accuracy of the result since it was not considered. The system sensitivity to ground displacement in 3 dimensions can be derived from Eq. (6):

$$\begin{bmatrix} u_U \\ u_E \\ u_N \end{bmatrix} = \begin{bmatrix} \cos(\theta) \\ -\sin(\theta)\ \cos(\alpha) \\ \sin(\theta)\ \sin(\alpha) \end{bmatrix} \tag{9}$$

where u_u, u_E, u_N denote the coefficient of Eq. (6). Given the satellite parameters for the ALOS PALSAR dataset used in this study, the coefficient vector $[\,u_u \quad u_E \quad u_N\,]^T$ is approximately equal to $[\,0.78 \quad -0.62 \quad -0.11\,]^T$. This suggested that an easterly displacement of 10 mm/year can result in displacement error of approximately 8 mm/year in vertical direction if the LoS displacement was directly projected into the vertical direction. The accuracy of vertical displacement measured from PSI can be enhanced if an additional ALOS PALSAR dataset acquired with descending orbit is available (Ng et al., 2011; Wright et al., 2004).

6.1.4. Poor temporal overlap between the datasets

The GPS-measured vertical displacement rates were estimated from only 4 GPS surveys. The estimated vertical displacement rates could be strongly influenced because of the possibly large temporal variations in the rates of subsidence. On the other hand, the PSI-measured vertical displacement rates were estimated from 17 ALOS PALSAR images. The vertical displacement rates of both measurements were estimated with different acquisition dates and different number of observations. These could lead to dispersion between estimated vertical displacement rates by both techniques (Section 5.2).

It can be seen in Fig. 7 that the data acquisition date for the ALOS PALSAR images and GPS surveys are not ideal for comparison. Therefore interpolation error is expected to be one of the reasons for the dispersion observed between both techniques in Section 5.3. In fact, the largest differences between the PSI-interpolated displacement and the GPS-measured displacement have been observed at the last GPS survey date where there was no ALOS PALSAR acquisition near that date (e.g. "MUBA", "KUNI", "T002" and "ANBA" in Fig. 7).

6.1.5. Mismatch in target points between the two techniques

The GPS surveys carries out measurement at the specific points (i.e. the survey marks) while the PSI-derived deformation represents the deformation of the dominant scatterer in the specific imaged pixel (i.e. the persistent scatterer). If the point of the GPS measurement is not the most dominant backscatter in the imaged pixel, then the deformation of such a point cannot be mapped by the PSI. If that point does not share the common deformation signal with its surrounding, it is possible there is some difference between the two measurements. It is expected to be the reason for the large dispersion between both techniques at the two GPS stations "KLGD" and "439B". In addition, the uncertainties in the geolocation for the PS points and GPS stations might cause mismatch in target points. This is why radar corner reflectors have been collocated with GPS monuments in some studies.

6.2. PSI to complement the GPS surveying technique for monitoring land subsidence in Jakarta

It can be seen by comparing Figs. 3 and 5 that PSI can provide deformation measurement in much higher spatial density in the case of Jakarta land subsidence monitoring. The high-spatial

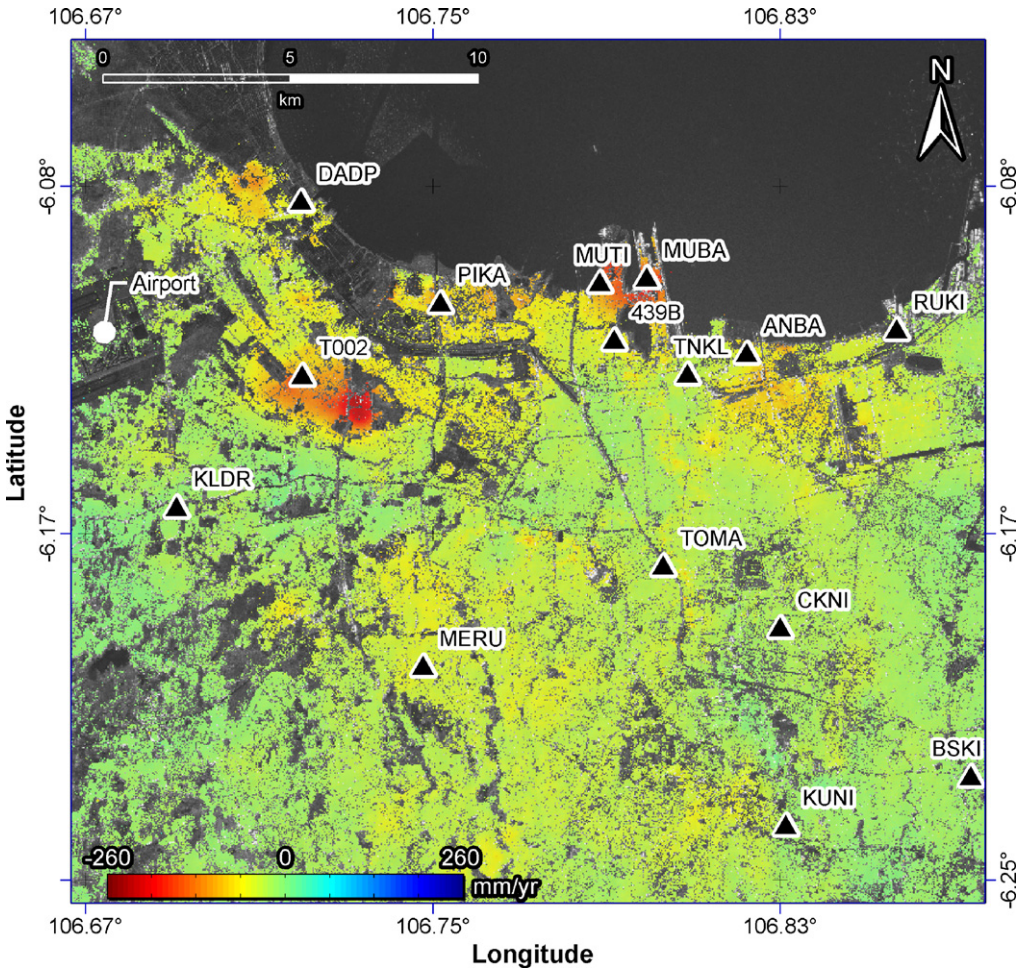

Fig. 9. The close-up image of the PSI-measured subsidence rate map superimposed on the SAR intensity image of northern Jakarta. The black triangle represents the location of the GPS stations.

density measurements from PSI allowed the land subsidence phenomenon in Jakarta to be better understood. The PSI results show that the whole Jakarta City was sinking. The measured average subsidence rate for Jakarta City was in general about 38 mm/year (with respect to the GPS station "BAKO") corresponding to 139 mm over the SAR acquisition period (1334 days). Fig. 9 shows a close-up image of the two obvious subsidence bowls from Fig. 3 around Mutiara and Cengkareng. The "Mutiara" subsidence bowl is located in Pantai Mutiara housing complex on a beach reclamation area. Two GPS stations, "MUTI" and "MUBA", are located close to the centre of the subsidence bowl. Unfortunately this is not the case for the "Cengkareng" subsidence bowl. The subsidence bowl located between Kalideres and Cengkareng is the settlement area surrounded by the international airport and industrial area. It can be seen from Fig. 9 that the closest GPS station ("T002") is at some distance to the centre of the subsidence bowl. This shows that the real subsidence phenomenon over Jakarta has been significantly underestimated by the GPS survey only. On the other hand, the spatial extent as well as the magnitude of the subsidence bowls can be clearly identified from the PSI-measured subsidence rate map in the majority of the area in Jakarta. This suggests that PSI can be used to complement the GPS surveying over Jakarta. The survey points for future GPS surveys can be planned based on the PSI-measured subsidence rate map. For example, the GPS surveys can be carried out at the centre of the subsidence bowl identified from PSI-measurement or in area where little/no PS can be identified. Therefore, by combining the GPS and PSI measurements, a more complete subsidence phenomenon over the whole Jakarta can be identified.

The PSI-measurement provides better temporal resolution than the GPS surveys in Jakarta between 2006 and 2010 (Fig. 7). It is more difficult to analyse the seasonal displacements from pure GPS surveys in Jakarta due to its low temporal sampling rate. The seasonal displacement is essential as it provides useful information for the hydrogeological assessment, groundwater extraction management as well as aquifer storage and recovery management. In the case of Jakarta, PSI-measurement provided land deformation measurement with higher temporal sampling allows seasonal displacements to be observed in Jakarta City. The temporal sampling rate of the deformation measurement can be further improved by combining the displacement values obtained from both techniques (see Fig. 7) and hence a more detailed displacement time series can be obtained. Therefore, the displacement measured from both techniques can not only be used to validate each other, but also be combined for better land subsidence analysis in both spatial and temporal domains.

7. Concluding remarks

In this study, the land subsidence in the Jakarta City, Indonesia mapped by GEOS-PSI has been presented. GEOS-PSI uses an adaptive estimation strategy that improves the quality of the PS results as well as maximises the pixel density. The elevation-related atmospheric signals are also considered in GEOS-PSI. The land

subsidence in Jakarta City and its surrounding were measured using 17 ALOS PALSAR radar images acquired between 31 January 2007 and 26 September 2010. Two obvious subsidence bowls with a maximum subsidence rate of 260 mm/year were identified in northern Jakarta.

Comparisons between the PSI-measurement and GPS-measurement have been carried out. Good correlation has been observed between displacements obtained from both techniques. The subsidence rate differences between the GPS-measurement and the PSI-measurement vary from −29 mm/year to 38 mm/year with average absolute difference of 11 mm/year and standard deviation of 16 mm/year. By considering 2 of the GPS stations as outliers, the average absolute subsidence rate differences between both measurements has improved to 8 mm/year and the standard deviation to 9 mm/year.

This study has demonstrated that PSI-measurement can provide reasonable temporal resolution with large spatial coverage/density compared to the campaign GPS surveying in Jakarta and hence can be used to complement the GPS surveying for monitoring land subsidence in Jakarta.

Acknowledgements

This research work has been partly funded by Australian Department of Resources, Energy and Tourism, Australian Research Council, the Cooperative Research Centre, the Australian Coal Association Research Program and the Chinese Ministry of Science and Technology. The authors wish to thank the Earth Remote Sensing Data Analysis Center (ERSDAC) for providing the ALOS PALSAR data. METI and JAXA retain ownership of the ALOS PALSAR original data.

References

Abidin, H., Andreas, H., Gumilar, I., Fukuda, Y., Pohan, Y., Deguchi, T., 2011. Land subsidence of Jakarta (Indonesia) and its relation with urban development. Natural Hazards, 1–19.

Abidin, H.Z., Andreas, H., Djaja, R., Darmawa, D., Gamal, M., 2008. Land subsidence characteristics of Jakarta between 1997 and 2005, as estimated using GPS surveys. GPS Solutions 12 (1), 23–32.

Abidin, H.Z., Djaja, R., Andreas, H., Gamal, M., Hirose, K., Maruyama, Y., 2004. Capabilities and constraints of geodetic techniques for monitoring land subsidence in the urban areas of Indonesia. Geomatics Research Australasia 81, 45–58.

Abidin, H.Z., Djaja, R., Darmawan, D., Hadi, S., Akbar, A., Rajiyowiryono, H., Sudibyo, Y., Meilano, I., Kusuma, M.A., Kahar, J., Subarya, C., 2001. Land subsidence of Jakarta (Indonesia) and its geodetic monitoring system. Natural Hazards 23 (2), 365–387.

Chen, Q., Liu, G., Ding, X., Hu, J.-C., Yuan, L., Zhong, P., Omura, M., 2010. Tight integration of GPS observations and persistent scatterer InSAR for detecting vertical ground motion in Hong Kong. International Journal of Applied Earth Observation and Geoinformation 12 (6), 477–486.

Colesanti, C., Ferretti, A., Novali, F., Prati, C., Rocca, F., 2003. SAR monitoring of progressive and seasonal ground deformation using the permanent scatterers technique. IEEE Transactions on Geoscience and Remote Sensing 41 (7), 1685–1701.

Costantini, M., Rosen, P.A., 1999. A generalized phase unwrapping approach for sparse data. In: IGARSS 1999, Hamburg, Germany, 28 June–2 July, pp. 267–269.

Farina, P., Colombo, D., Fumagalli, A., Marks, F., Moretti, S., 2006. Permanent scatterers for landslide investigations: outcomes from the ESA-SLAM project. Engineering Geology 88 (3–4), 200–217.

Ferretti, A., Prati, C., Rocca, F., 2000. Nonlinear subsidence rate estimation using permanent scatterers in differential SAR interferometry. IEEE Transactions on Geoscience and Remote Sensing 38 (5), 2202–2212.

Ferretti, A., Prati, C., Rocca, F., 2001. Permanent scatterers in SAR interferometry. IEEE Transactions on Geoscience and Remote Sensing 39 (1), 8–20.

Fialko, Y., Simons, M., Agnew, D., 2001. The complete (3-D) surface displacement field in the epicentral area of the 1999 Mw 7.1 Hector Mine Earthquake, California, from space geodetic observations. Geophysical Research Letters 28 (16), 3063–3066.

Ge, L., Chang, H.C., Rizos, C., 2007. Mine subsidence monitoring using multi-source satellite SAR images. Photogrammetric Engineering and Remote Sensing 73 (3), 259–266.

Hanssen, R.F., 2001. Radar Interferometry – Data Interpretation and Error Analysis. Kluwer Academic Publishers, The Netherlands, 328 pp.

Hooper, A.J., 2006. Persistent scatterer radar interferometry for crustal deformation studies and modelling of volcanic deformation. PhD Thesis. Department of Geophysics, Stanford University, USA, 124 pp.

Jiang, L., Lin, H., 2010. Integrated analysis of SAR interferometric and geological data for investigating long-term reclamation settlement of Chek Lap Kok Airport, Hong Kong. Engineering Geology 110 (3–4), 77–92.

Kampes, B., Hanssen, R.F., 2004. Ambiguity resolution for permanent scatterer interferometry. IEEE Transactions on Geoscience and Remote Sensing 42 (11), 2446–2453.

Kampes, B.M., 2005. Displacement parameter estimation using permanent scatterer interferometry. PhD Thesis. Delft University of Technology, Delft, The Netherlands, 168 pp.

Kampes, B.M., 2006. Radar Interferometry: Persistent Scatterer Technique. Springer, Dordrecht, 211 pp.

Kumar, V., Venkataramana, G., Høgda, K.A., 2011. Glacier surface velocity estimation using SAR interferometry technique applying ascending and descending passes in Himalayas. International Journal of Applied Earth Observation and Geoinformation 13 (4), 545–551.

Lanari, R., Lundgren, P., Sansosti, E., 1998. Dynamic deformation of Etna volcano observed by satellite radar interferometry. Geophysical Research Letters 25, 1541–1544.

Massironi, M., Zampieri, D., Bianchi, M., Schiavo, A., Franceschini, A., 2009. Use of PSInSAR(TM) data to infer active tectonics: clues on the differential uplift across the Giudicarie belt (Central-Eastern Alps, Italy). Tectonophysics 476 (1–2), 297–303.

Massonnet, D., Rossi, M., Carmona, C., Adragna, F., Peltzer, G., Fiegl, K., Rabaute, T., 1993. The displacement field of the Landers earthquake mapped by radar interferometry. Nature 364, 138–142.

Murdohardono, D., Sudarsono, U., 1998. Land subsidence monitoring system in Jakarta. In: Proceedings of Symposium on Japan – Indonesia IDNDR Project: Volcanology, Tectonics, Flood and Sediment Hazards, Bandung, 21–23 September, pp. 243–256.

Murdohardono, D., Tirtomihardjo, H., 1993. Penurunan Tanah di Jakarta dan rencana pemantauannya. In: Proceedings of the 22nd Annual Convention of the Indonesian Association of Geologists, Bandung, 6–9 December, pp. 346–354.

Ng, A.H.-M., Chang, H.C., Ge, L., Rizos, C., Omura, M., 2009. Assessment of radar interferometry performance for ground subsidence monitoring due to underground mining. Earth, Planets and Space 61 (6), 733–745.

Ng, A.H.-M., Ge, L., Yan, Y., Li, X., Chang, H.C., Zhang, K., Rizos, C., 2010. Mapping accumulated mine subsidence using small stack of SAR differential interferograms in the Southern coalfield of New South Wales, Australia. Engineering Geology 115 (1–2), 1–15.

Ng, A.H.-M., Ge, L., Zhang, K., Chang, H.C., Li, X., Rizos, C., Omura, M., 2011. Deformation mapping in three dimensions for underground mining using InSAR – Southern Highland coal field in New South Wales, Australia. International Journal of Remote Sensing 32 (22), 7227–7256.

Ng, A.H.-M., Ge, L., Zhang, K., Li, X., 2012. Monitoring ground deformation in Beijing, China with Persistent Scatterer SAR Interferometry. Journal of Geodesy, doi:10.1007/s00190-011-0525-4.

Osmanoglu, B., Dixon, T.H., Wdowinski, S., Cabral-Cano, E., Jiang, Y., 2011. Mexico City subsidence observed with persistent scatterer InSAR. International Journal of Applied Earth Observation and Geoinformation 13 (1), 1–12.

Primanita, A., 2010. Jakarta Areas Muara Baru, Cengkareng Sinking Fast. Jakarta Globe, Jakarta.

Rimbaman, Suparan, P., 1999. Geomorphology. In: Proceeding of COASTPLAN JAKARTA BAY PROJECT, Coastal Environmental Geology of the Jakarta Reclamation Project and Adjacent areas., CCOP COASTPLAN Case Study Report No. 2, Jakarta/Bangkok, pp. 21–25.

Setiawati, I., 2010. After Census City Plans for 9.5 Million. The Jakarta Post, Jakarta.

Tukey, J.W., 1977. Exploratory Data Analysis. Addison-Wesley, Reading, USA.

Wright, T.J., Parsons, B.E., Lu, Z., 2004. Toward mapping surface deformation in three dimensions using InSAR. Geophysical Research Letters 31 (1), L01607.1–L01607.5.

Zebker, H.A., Rosen, P.A., Goldstein, R.M., Gabriel, A.K., Werner, C.L., 1994. On the derivation of coseismic displacement-fields using differential radar interferometry – the Landers Earthquake. Journal of Geophysical Research 99 (B10), 19617–19634.

Zhang, K., Ng, A.H.-M., Ge, L., Dong, Y., Rizos, C., 2010. Multi-path PALSAR interferometric observations of the 2008 magnitude 8.0 Wenchuan earthquake. International Journal of Remote Sensing 31 (13), 3449–3463.